Tissue Properties Estimation Inverse Finite Element Method

Authors:
Carlos Eduardo
Ribeiro Santa Cruz Mendoza

Supervisor:
Alberto
García González

July 23, 2019

1 Introduction

Characterizing the mechanical properties of living tissues has for long been of major importance for clinical medicine. A clear reason for that is the transition of the these properties as the tissue becomes cancerous, facilitating diagnoses through palpation and other means [1]. On the other hand, for surgical medicine, the widening in the material property spectrum makes the planning and action of the surgery more arduous. The unpredictability of the tissue response as it's manipulated raises the chance of mistakes in procedures that could already be difficult due to complicated access, for example.

Most recently, with the ongoing development of 3D-printing, surgical training with 3-D printed replicas are becoming a reality. Thus, the fair characterization of the material properties is again crucial to provide the surgeons a comparable experience [2].

Under this context, the present work aims on providing an algorithm to extract the material properties of the tissue to be manipulated using simple indentation tests made on the target and the geometry as inputs. From the force response of the indentation test, the algorithm applies the so called "Inverse Finite Element Method" to provide the required parameters for the 3D-printing of the training models.

1.1 Tumor Properties

The general clinical description of tumors is that it's usually stiffer than the normal tissue from which it arose [1]. One of the reasons this might happen is the abnormal communication of a cancer cell to it's environment. The extracellular matrix (ECM), a network on the vicinity of the cell composed by collagen, enzymes and glycoproteins among other macromolecules, sustains the cell both structurally and biochemically [3]. In the presence of cancer, the signaling in and out of the cell is affected, resulting in the stiffening of the ECM. On the other hand, a stiffer environment affects the motility and proliferation of the cells, completing a feedback loop that elevates the spreading danger of a tumor and, thus, a stiffening of the tissue [1].

The stiffening of the ECM comes partially from the imbalance of the production and degradation of its proteins, which leads to deposition of collagen. However, although the tissue as a whole stiffens with the presence of cancer, malignant cells are generally softer.

1.2 Healthy and cancerous tissue properties

Biological tissues are complicated to describe, given that, not only they're extremely diverse, but also their mechanical properties depend on time (strain rate, age of tissue),

moisture and often change after death [4].

Fung (1981)[5] provides a comprehensive theory on bioviscoelastic solids and a relevant compilation on mechanical properties and the nonlinear relationship between stress and strain for several different (healthy) tissues. One example is the heart muscle, from which the tensile test is presented on Figure 1.1a.

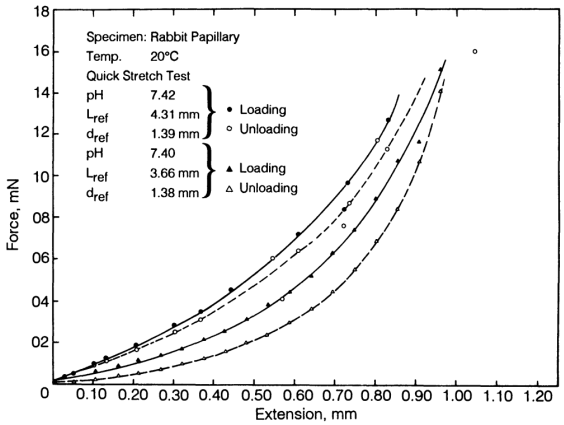

(a) Tensile test response of the papillary muscle of a rabbit's heart. Circular dots refer to "high speed" tests as for the triangles refer to loading and unloading at small constant rates

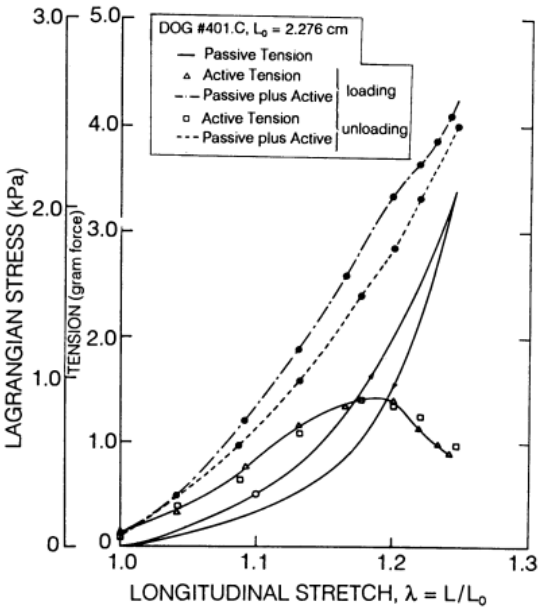

(b) Loading and unloading on ureter muscle under the "passive" and "active" states

Figure 1.1: Peculiar tissue responses [5]

As we can see, the tissue is rate dependent, presents a nonlinear elastic behaviour and follows different paths under loading and unloading. Some tissues as the striated muscles also present the "passive" and "active" variables. The contractile fibers can alter significantly the response to mechanical action such as illustrated on Figure 1.1b. Bones, on the other hand, behave similarly to many engineering materials. It has an linear elastic behaviour as seen on Figure 1.2 (17.5 to 18.9 GPa Elastic Modulus on humans) and is relatively brittle, specially in its dry form (fails at 0.4% strain, while wet bone fails at 1.2).

Krouskop *et. al* (2013)[4] presents data on healthy and cancer tissues of breast and prostate. Several samples were submitted to compression tests and showed the strong nonlinearity of the elastic response of living tissues, specially for cancerous ones. The elastic modulus is low at low strain but grows rapidly for higher strain levels, as Figure 1.3 shows. At a compressed stage, cancerous tissues were found to be to be up to ten times stiffer than the surrounding tissues such as fat.

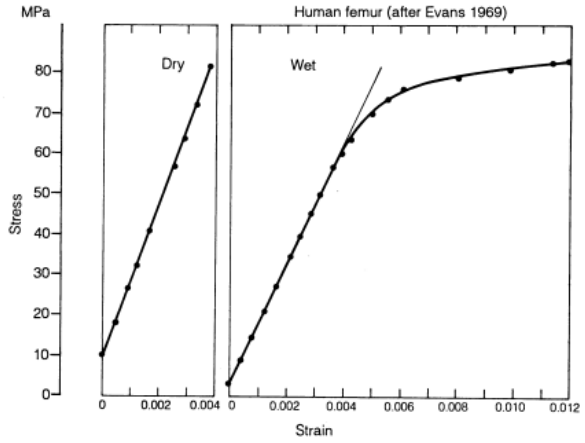

Figure 1.2: Stress-strain curve for human femoral bone [5]

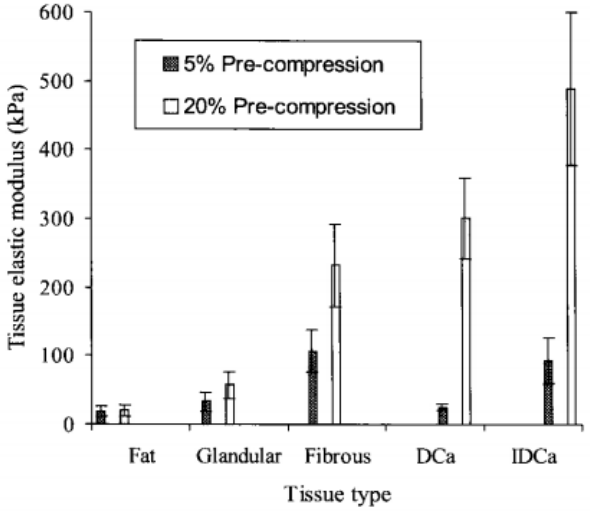

Figure 1.3: Dependence on Pre-Compression for different tissues (DCa = Ductal Carcinoma, IDCa = Invasive and Infiltrating ductal carcinoma). [4]

2 Inverse Finite Element Method

As shown on section 1.2, living tissues present themselves in a wide variety of mechanical properties. Evidently, simplifications are required to model such materials.

According to Liu *et. al* [6], it's valid to assume the hypothesis of incompressibility (Poisson $\nu \approx 0.5$) and homogeneity when characterizing solid organs. Soft tissues (such as fat, skin, kidney, liver and other organs) are also modelled as hyperelastic via strain

energy functions such as the Arruda-Boyce.

With the given assumptions, the tissue (or combination of tissues) can be modeled aiming to replicate the results from experimental data obtained from the real tissue. The inverse Finite Element Method is an algorithm that attempts exactly that. That is, instead of solving for forces or displacements given material properties, the properties themselves are determined by iteratively minimizing the difference between simulation and experiment.

2.1 Arruda-Boyce Hyperelastic Model

Following the procedure on [6, 7, 8], the chosen hyperelastic strain energy function was the Arruda-Boyce (AB) model given in Equation 2.1 (already considering incompressibility).

$$W = \mu \sum_{i=1}^{5} \frac{C_i}{\tau_m^{2i-2}} (I_1^i - 3^i) \tag{2.1}$$

where $I_1 = \sqrt{(\lambda^2 + \frac{2}{\lambda})}$, $\tau_{\text{chain}} = \sqrt{\frac{1}{3}(\lambda^2 + \frac{2}{\lambda})}$, $C_1 = 1/2$, $C_2 = 1/20$, $C_3 = 11/1050$, $C_4 = 19/7000$ and $C_5 = 519/673750$. τ_m is equal to the chain stretch at which the stress increases dramatically with the deformation and μ is the shear modulus.

As stated, the inverse method aims to find the material parameters to match the response of the finite element model with the experiment. In the case of the AB model, the chosen parameter to be iteratively updated is the shear modulus μ (the locking stretch is assumed to be constant).

2.2 Iteration under Newton-Raphson

The first step of the method is to run the simulation with an arbitrary initial parameter to compare the response with the experimental data. The comparison is made between force-displacement plots via squared difference:

$$e_k = \frac{1}{n} \sum_{i=1}^{n} (\boldsymbol{F}_{m_i} - \boldsymbol{F}_{FE_i}^k)^2 \tag{2.2}$$

where n is the number of experimental points (the FE response is interpolated to provide data at the same displacement points), F_{m_i} is the experimental response, F_{FE_i} is the finite element response and k is the current iteration step.

According to the Newton-Raphson method the new parameter μ can be calculated as follows:

$$\mu_{k+1} = \mu_k - J^{-1} e_k \tag{2.3}$$

where J would be the jacobian of the function. However, the jacobian takes no analytical form for the FE method, thus an approximation is inserted in the equation, with α being set to 1 for uniaxial indentation and 0.5 for rolling indentation.

$$\mu_{k+1} = \mu_k - \alpha\left(\frac{\mu_k - \mu_{k-1}}{e_k - e_{k-1}}\right)e_k \tag{2.4}$$

3 Uniaxial indentation

The test of uniaxial indentation can be used in combination with the inverse FE method to obtain properties of single tissues. The present chapter is based on the work of Sangpradit (2013) [9].

3.1 Experiment

The experimental data is drawn from a simple indentation test as presented on Figure 3.1. The reaction force on the indenter is measured and plotted against the axial displacement of the spherical wheel. The tested material is a cube of 15x15x15 mm^3 made of silicone (RTV 6166, General Electric, $\mu = 1300$), which is said to have similar mechanical properties as some biological tissues.

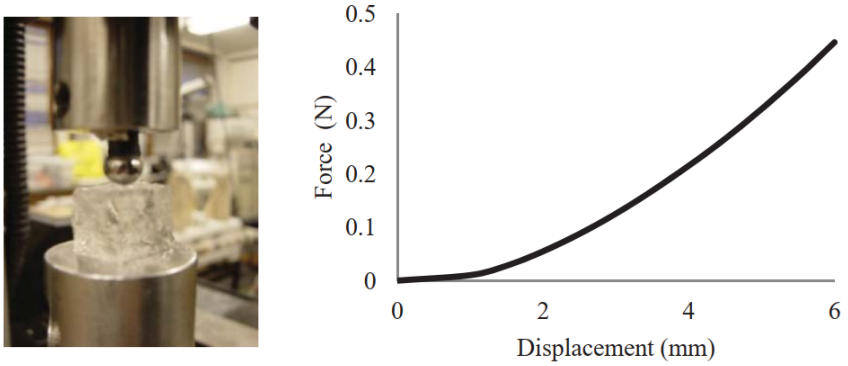

(a) (b)

Figure 3.1: The experiment (a) and it's response (b). Indentation: Spherical wheel with 8 mm in diameter at INSTRON 5565 machine. Measurement: ATI Nano17 force sensor (resolution = 0.003 N, sampling rate = 100 Hz)

3.2 Model

The 3D model of the silicone was assumed to be **incompressible** and **homogeneous**. The selected strain energy function to feed the hyperelastic model was the Arruda Boyce (AB). The indenter on the other hand was considered to be "discrete rigid" with 8 mm of diameter.

The interaction between both parts is set as a surface to surface contact in which the indenter goes 6 mm deep at the center of the silicone probe. The contact is **frictionless**.

Naturally, the bottom of the silicone was fixed to the ground. A reference point was located on the center of the indenter sphere and assigned a vertical displacement of 6 mm downward, to be made in 1 second. At the same reference point, the reaction force was later analysed.

The indenter was meshed with 568 R3D3 rigid elements, while the cube was meshed with 1000 elements of 8-node linear brick, reduced integration and hourglass control C3D8R.

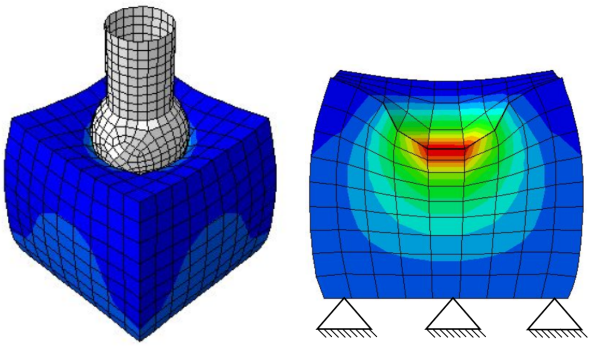

(a) (b)

Figure 3.2: Isometric (a) and cut (b) view of the indentation.

3.3 Results

Once the model was developed, a Matlab/Unix code was written to automatically run the simulation, initially with a user-defined shear modulus, and perform all the steps explained on chapter 2. The code performed well and was able to converge the shear modulus to a value quite close to the real one, as it can be seen on Figure 3.3.

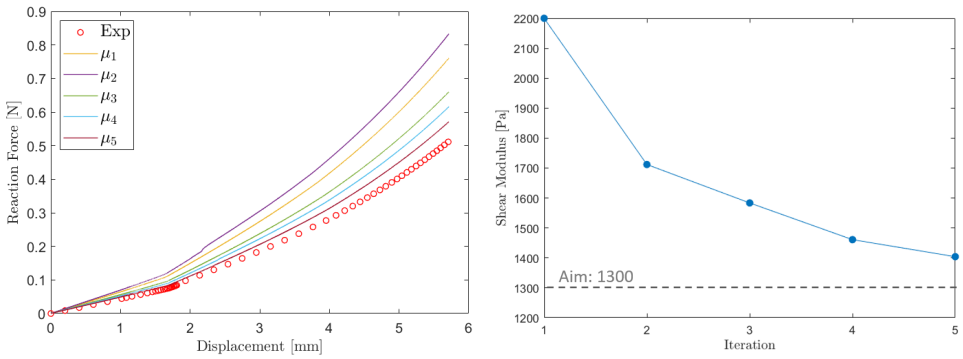

(a) (b)

Figure 3.3: Force-displacement curves for each iteration and experimental data (a) and shear modulus convergence (b). Initial data was $\mu_0 = 2000$ and $\mu_1 = 2200$

4 Rolling Indentation

The rolling indentation test aims to discover the properties of a material embedded in another one. Ultimately, this could allow tumors to be characterized while still inside another tissue. The present chapter is based on [6, 7, 9].

4.1 Experiment

The experimental data is drawn similarly from the uniaxial indentation. However, once the indenter has reached the desired depth in the tissue, it starts rolling sideways until it has swiped the whole length of the tissue. This allows us to analyse the measurement response in respect to the horizontal displacement of the indenter. The presence of another tissue, with different properties, express itself by a peak (or valley) in the reaction force plot. The experimental setup and corresponding measurement is shown on Figure 4.1

On the presented case, the used materials simulating tissue and tumors are a block (30x150x50 mm^3) of silicone and three small cylinders (10mm of diameter, 20mm of height). Both of them are modeled via the AB model with $\mu = 4980$ and $\mu = 73400$ for the silicone and rubber respectively.

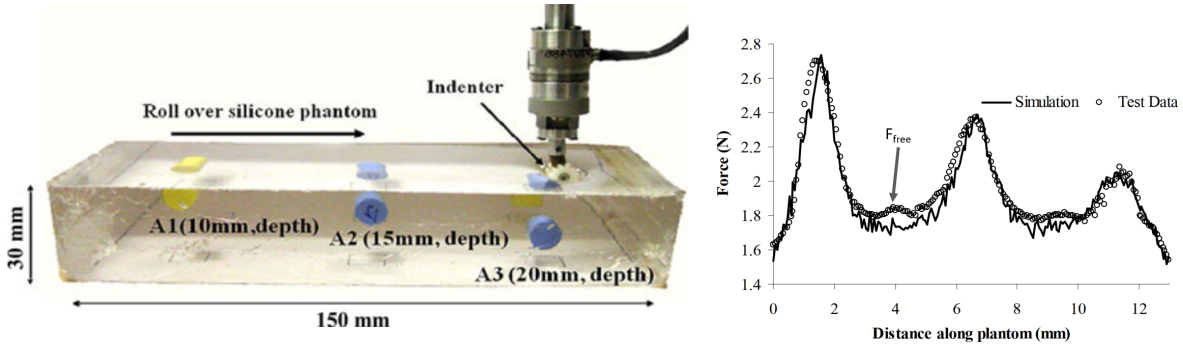

(a) (b)

Figure 4.1: Experimental setup (a) and Reaction force measurement (b)

4.2 Model

The 2D model maintained most of the characteristics of the uniaxial indentation model. That is, incompressible and homogeneous materials, a discrete rigid indenter of 8 mm, a frictionless contact between the indenter and the silicone and a fixed bottom of the silicone sample.

The simulation is done in two steps, first the indenter reaches the desired depth (constrained at every direction except from the downward movement) and then moves laterally. A lateral velocity (and a correspondent rotational velocity to prevent sliding) was assigned to the indenter in the second step, allowing it to run the whole lenght in 1 second (different velocities did not alter the result, due to the not introduction of viscous effects).

The probe was modeled as a reduced version of the one presented on Figure 4.1. A length of 100mm was modeled contemplating the last two embedded cylinders. The silicone was, thus, modelled as a rectangle with two holes, whereas the tumors were represented by circles. The interaction between silicone and tumors was set as a "tie interaction", in which the surfaces in contact are tied, meaning the "shared" nodes must move equally.

The indenter was meshed with 32 R2D2 rigid elements, the silicone was meshed with 5066 elements of four-node bilinear plane stress quadrilateral elements CPS4R and the tumors were meshed with 181 elements of the same type each.

4.3 Results

The Matlab/Unix code was, then, adapted to the rolling indentation model. The new algorithm differentiate itself from the uniaxial indentation one basically on the error function. According to Liu *et. al* (2014), for the rolling indentation, a better suited error function states:

$$e_k = |\max(\boldsymbol{F}_{FE_k} - \boldsymbol{F}_{free}) - \max(\boldsymbol{F}_M - \boldsymbol{F}_{free}) \tag{4.1}$$

where $\boldsymbol{F}_{free}$ is the force response considering no embedded tumors, that is, as if the probe was made exclusively of silicone (with no holes in it).

This way, the subject of comparison is solely the peak of each curve. This avoids divergence problems caused by some significant differences between model and experiment given by surface geometry and indentation path irregularities.

Again, the code performed well as was able to reach the desired value in a few iterations. Figure 4.2 depicts the model and shows the reaction force felt by the indenter at each horizontal position.

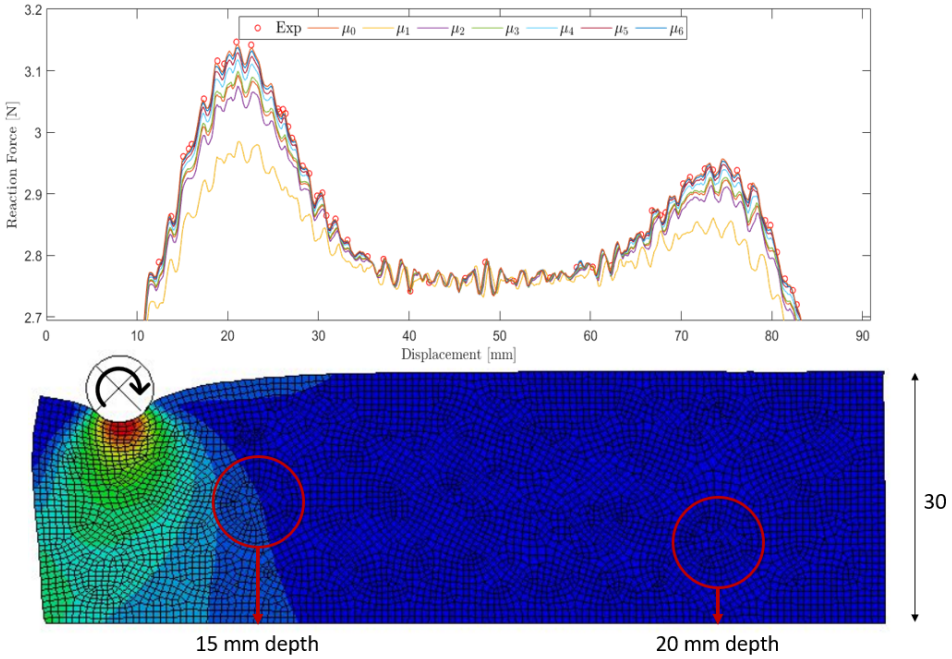

Figure 4.2: Rolling indentation model results. Initial data $\mu_0 = 50000$ and $\mu_1 = 30000$

The convergence and a better look at the peak caused by the tumor's presence can be seen in Figure 4.3

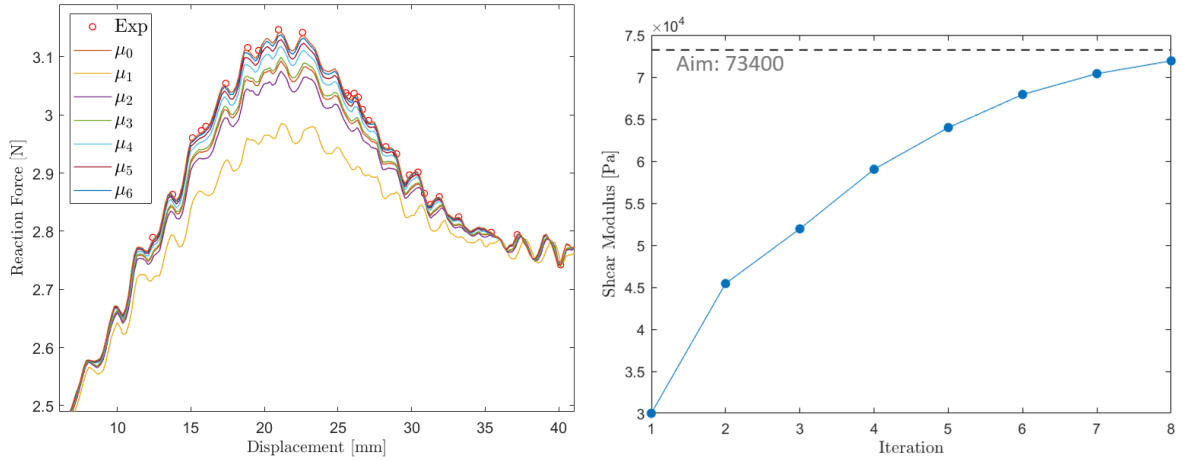

(a) (b)

Figure 4.3: Reaction force at tumor position (a) and Convergence of shear modulus (b)

However, for the rolling indentation, it can only be said that it qualitatively matches the experiment. The "experimental points" used to test the algorithm were actually drawn from a simulation of the model using the desired shear modulus. The real experimental points couldn't be used due to the difference between the experimental and

simulated $\boldsymbol{F}_{free}$ reaction forces. As it can be seen on Figure 4.4, the simulated $\boldsymbol{F}_{free}$ is almost 1N higher than the obtained on the article, forbidding the comparison to be made between the peaks.

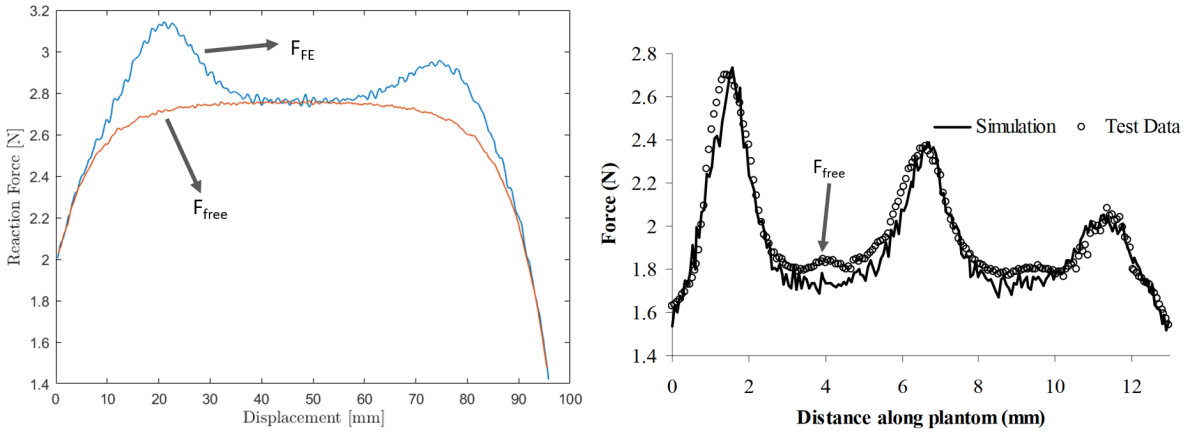

(a) (b)

Figure 4.4: Simulation (a) Article data (b)

5 Conclusion

The inverse Finite Element Method has proven to be a powerful tool in enabling characterization of materials of difficult access. The good results obtained in simple models and the agreement already obtained in real organ studies such as from Liu *et. al* (2014), prove that this method could be an ally in surgery planning in the future. The main difficulties, however, lie on the fact that it's still quite restrictive on tissue kinds. As we've seen, several tissues present characteristics such as anisotropy that cannot be ignored. Additionally, tumors are also known to change their properties once strained to a certain level [4] and the sensitivity of methods such as the one presented in chapter 4 is limited. If the tumor is somewhat deep, the method could prove to be useless (more than 2.5cm below surface). Furthermore, the challenge lies as well in the capability of a printed material to replicate hyperelastic properties. Thus, further investigation is needed to provide a reliable method for surgeons to apply on a daily basis.

Bibliography

[1] Cheng Dong, Nastaran Zahir, and Konstantinos Konstantopoulos. *Biomechanics in Oncology*, volume 1092. 2018.

[2] C Lee Ventola. Medical applications for 3d printing: Current and projected uses. *P T : a peer-reviewed journal for formulary management*, 39(10):704—711, October 2014.

[3] Achilleas D. Theocharis, Spyros S. Skandalis, Chrysostomi Gialeli, and Nikos K. Karamanos. Extracellular matrix structure. *Advanced Drug Delivery Reviews*, 97:4 – 27, 2016. Extracellular Matrix (ECM) and ECM-like materials: Therapeutic Tools and Targets in Cancer Treatment.

[4] Brian S. Garra, Faouzi Kallel, Thomas M. Wheeler, Thomas A. Krouskop, and Timothy Hall. Elastic Moduli of Breast and Prostate Tissues under Compression. *Ultrasonic Imaging*, 20(4):260–274, 2013.

[5] Y C Fung. *Mechanical properties of living tissues.* 1981.

[6] Hongbin Liu, Kiattisak Sangpradit, Min Li, Prokar Dasgupta, Kaspar Althoefer, and Lakmal D. Seneviratne. Inverse finite-element modeling for tissue parameter identification using a rolling indentation probe. *Medical and Biological Engineering and Computing*, 52(1):17–28, 2014.

[7] Kiattisak Sangpradit, Hongbin Liu, Prokar Dasgupta, Kaspar Althoefer, and Lakmal D. Seneviratne. Finite-element modeling of soft tissue rolling indentation. *IEEE Transactions on Biomedical Engineering*, 58(12 PART 1):3319–3327, 2011.

[8] K. Sangpradit, H. Liu, L. D. Seneviratne, and K. Althoefer. Tissue identification using inverse finite element analysis of rolling indentation. In *2009 IEEE International Conference on Robotics and Automation*, pages 1250–1255, May 2009.

[9] K. Sangpradit. Parameter estimation for a mechatronic probe of robot assisted minimally invasive surgery using inverse finite element analysis. *Journal of Research and Applications in Mechanical Engineering*, 1(4):9–14, 2013.